

Paradoxical effects for a one-dimensional periodic potential embedded in a two-dimensional systemKira Kolpatzeck, Lothar Brendel, and Rolf Möller *Fakultät für Physik, Universität Duisburg-Essen, Lotharstr. 1-21, 47048 Duisburg, Germany*Roberto Robles *Centro de Física de Materiales CFM/MPC (CSIC-UPV/EHU), 20018 Donostia-San Sebastián, Spain*

Nicolás Lorente

*Centro de Física de Materiales CFM/MPC (CSIC-UPV/EHU), 20018 Donostia-San Sebastián, Spain
and Donostia International Physics Center (DIPC), 20018 Donostia-San Sebastián, Spain*

(Received 23 December 2022; revised 1 March 2023; accepted 27 March 2023; published 14 April 2023)

The electronic state at the interface between the Ag(111) surface and NaCl island has been studied. Due to the lattice mismatch, islands of NaCl grow on Ag(111) with various moiré patterns which lead to a weak periodic one-dimensional (1D) potential for the electronic state. In contrast to the well-known situation for a purely 1D system, the ideal two-dimensional system should cause a modulation of the local electronic density for energies only below and not above the mini band gap corresponding to the periodic potential. However, the experimental observation by scanning tunneling microscopy and spectroscopy of states reveals such a modulation also in the forbidden range of energy. Since the particular system allows us to disentangle the effects of local scattering and those caused by the periodic potential, it could be revealed that the loss of coherence and the mechanism of the detection by the STM are responsible for the experimentally observed modulation, which should be suppressed in the case of an ideal system.

DOI: [10.1103/PhysRevB.107.155418](https://doi.org/10.1103/PhysRevB.107.155418)**I. INTRODUCTION**

The problem of a nearly free two-dimensional (2D) electron (NFE) gas subjected to a weak periodic potential is both of principal interest as well as of practical importance because there is a vast number of physical realizations [1–12]. It has been discussed theoretically for a long time, see, e.g., Ref. [1]. 2D electron systems have been intensively studied, for example, for the interfaces in semiconductor heterostructures. Atomically precise superstructures for such an interface state have been realized [4], discussing the prediction by the Kronig-Penney model [13]. NFE-type surface states are naturally found at several perfectly ordered crystal surfaces, e.g., for the noble metals Au(111), Ag(111), and Cu(111) [5–8]. Depending on the doping, 2D materials, like graphene or transition-metal dichalcogenides, may also exhibit a nearly free 2D electron gas [9]. Various one-dimensional (1D) or 2D periodic potentials may be imposed on perfect 2D systems by additional adlayers forming moiré patterns because of lattice mismatch, see, e.g., Refs. [10–12].

Whereas in early experiments using semiconductor heterostructures only the total electronic density as a function of energy could be measured directly, the invention of scanning tunneling spectroscopy allowed for the study of the local density of electronic states (LDOS) for electronic surface states and interface states in the vicinity of the surface [14]. As an example of a NFE with an intrinsic periodic modulation, the LDOS of the Au(111) surface with the well-known herringbone reconstruction has been studied by Fourier transform

scanning tunneling spectroscopy [15]. The technique works best if the observed modulations in the dI/dV measurements are only due to a modulation of the LDOS. For NaCl islands on the noble metals, Au(111) [16,17], Ag(111) [18,19], and Cu(111) [20] where the corrugation correlated to the modulation of the LDOS is well below a tenth of an Å interfering effects can be almost neglected. However, for a larger corrugation, e.g., for ordered layers of organic molecules on noble metals, a more sophisticated analysis is required [21–23].

The present paper deals with the interface state between a NaCl adlayer and Ag(111). Due to the lattice mismatch between the hexagonal surface structure of the Ag(111) and the quadratic one of the NaCl, the islands grow with a large commensurate supercell. The variation of the position of the sodium and chlorine atoms relative to the underlying silver atoms leads to a moiré pattern, which forms a 1D periodic potential for the 2D interface state. This particular system enables us to disentangle different effects leading to a modulation of the LDOS. The findings triggered a theoretical and numerical study of the problem, thus elucidating principal aspects and features of this kind of electronic system. Indeed, previous experiments describing the emerging electronic structure due to the interface-state modulations in MgO on Au(111) [24], NaCl on Ag(111) [18,19,25], and NaCl on Cu(111) [20] have been mainly explained using the text book models for a 1D electronic system under a weak periodic potential. However, the measured modulation of the LDOS with the period of the weak potential persists for energies well above the band gap opened by the 1D potential, contrary to the

model's prediction that there should be almost no modulation of the LDOS in that energy range at all. Our paper reveals that the experimental observations by us and other groups cannot be explained by applying the model of an ideal free 2D electron gas embedded in a 1D periodic potential. Only if the limited coherence of the involved electronic state and the detection mechanism by scanning tunneling spectroscopy are included, can the experimental findings be rationalized.

II. EXPERIMENT

Experimental details

The experiments as well as the sample preparation were carried out under ultrahigh vacuum conditions. The Ag(111) substrate surface was cleaned *in situ* by several cycles of Ar⁺-ion sputtering with a kinetic energy of 2.6 keV and a sputtering current density of $\sim 25 \frac{\mu\text{A}}{\text{cm}^2}$ for 30 min and annealing to 530 °C by thermal radiation for 10 min. Subsequently, NaCl was deposited onto the Ag(111) surface from a Knudsen cell operated at 565 °C while the sample was kept at ~ 40 °C. To control the evaporation rate, a quadrupole mass spectrometer was used.

The measurements shown in this paper were performed with a home-built low-temperature scanning tunneling microscope, working at 8 K, cooled by liquid helium. The bias voltage was applied to the sample while the tunneling current was measured at the tunneling tip. The electrolytically etched tungsten tips were cleaned under vacuum conditions by electron bombardment and field emission in front of a copper surface in the cold STM. The data were acquired by using the open-source software GXSM [26]. For further image processing, the software programs WSXM [27] and IMAGEJ [28] were used.

III. RESULTS

When NaCl layers grow on Ag(111), the square lattice aligns with one axis of the hexagonal lattice of the silver. However, a commensurate layer is not possible with the ideal and nondistorted lattices. For very small islands, the stress and strain can be accommodated. Extended areas form a superlattice with rather large commensurate supercells. Since not all the atoms of the NaCl layer are located in ideal positions on the substrate, a moiré pattern with parallel lines occurs. As can be seen in Fig. 1, several different patterns may be observed depending on the size, the aspect ratio, and the orientation of the islands. It should be noted that the corrugation observed in the topographic images is only about $\delta z_{p-p} = 0.015$ Å, which is very little compared to the height of the island of $\Delta z = 3.5$ Å [19]. Hence, a shaded representation of the data has been chosen to make the corrugation visible.

Figure 2 displays tentative models for islands I and II, indicating how the NaCl layer is arranged on the silver surface. It turns out that for most orientations of the NaCl islands, alternating stripes occur with the Cl⁻ and the Na⁺ ions resting either nearly on top or on a bridge position. The distance between the stripes may vary between about 20 Å and 30 Å. Figure 2(c) displays the hexagonal lattice of the silver and the square lattice of the NaCl. For the latter, both the primitive and commonly used $c(\sqrt{2}X\sqrt{2})$ unit cells are given. Please note

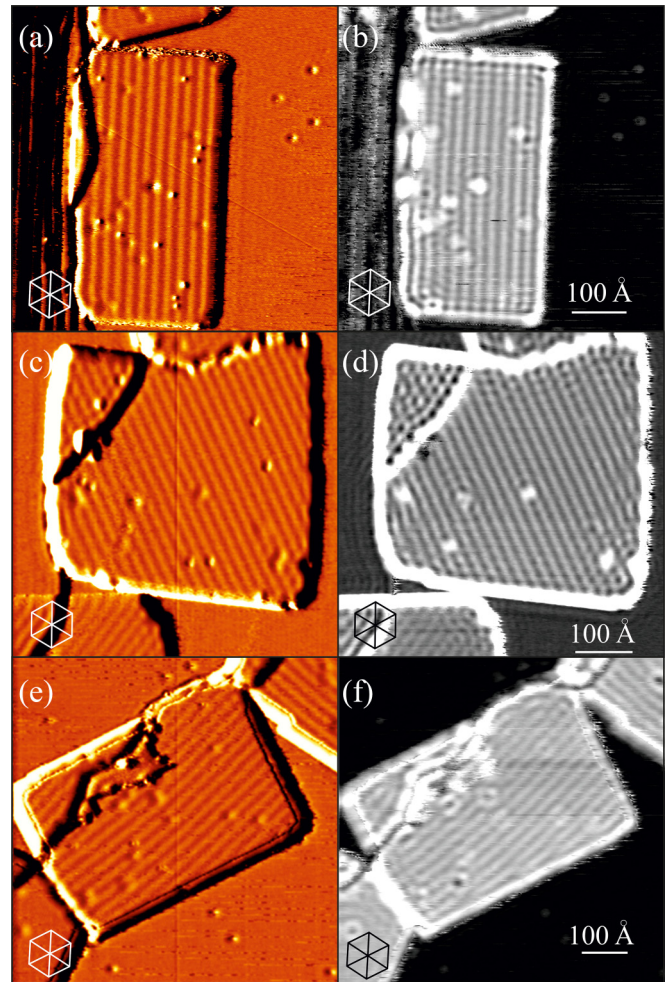


FIG. 1. Three different islands of NaCl on Ag(111) showing moiré patterns. The “star” in the lower left corner of each figure indicates the axes of the unit cell of the Ag(111) lattice. For each island, the orientation and the period of the stripe patterns is different. The left side displays topographic images, the right the corresponding dI/dV maps, which represent the LDOS for the given bias voltage which is applied to the sample. For the topographic images, a shaded representation has been chosen to emphasize the corrugation on the island, which is minute relative to the height of the NaCl islands. (a) Topography of island I, $U_t = 0.28\text{V}$ and $I_t = 500$ pA. (b) dI/dV map of island I, $U_t = 0.24\text{V}$, $I_t = 500$ pA, period $p = 22.5$ Å. (c) Topography of island II, $U_t = 0.33\text{V}$, $I_t = 500$ pA. (d) dI/dV map island II, $U_t = 0.30\text{V}$, $I_t = 500$ pA, period $p = 20.15$ Å. (e) Topography island III, $U_t = 0.22\text{V}$, $I_t = 800$ pA. (f) dI/dV map island III, $U_t = 0.25\text{V}$, $I_t = 800$ pA, period $p = 27$ Å.

that only the two adjacent layers at the interface are shown, although the NaCl islands are formed by a double layer. Moreover, the undistorted NaCl lattices without relaxation are drawn.

A tentative model for island I is obtained if the square lattice of the NaCl aligns with one axis of the Ag lattice. A $8\sqrt{2} \times \sqrt{2}$ supercell in terms of the quadratic NaCl lattice is formed, which is commensurate. This arrangement requires only a little relaxation with an expansion along the short axis of 2.3% and a compression of 0.3% along the long axis of the unit cell for the superstructure marked by the green rectangle

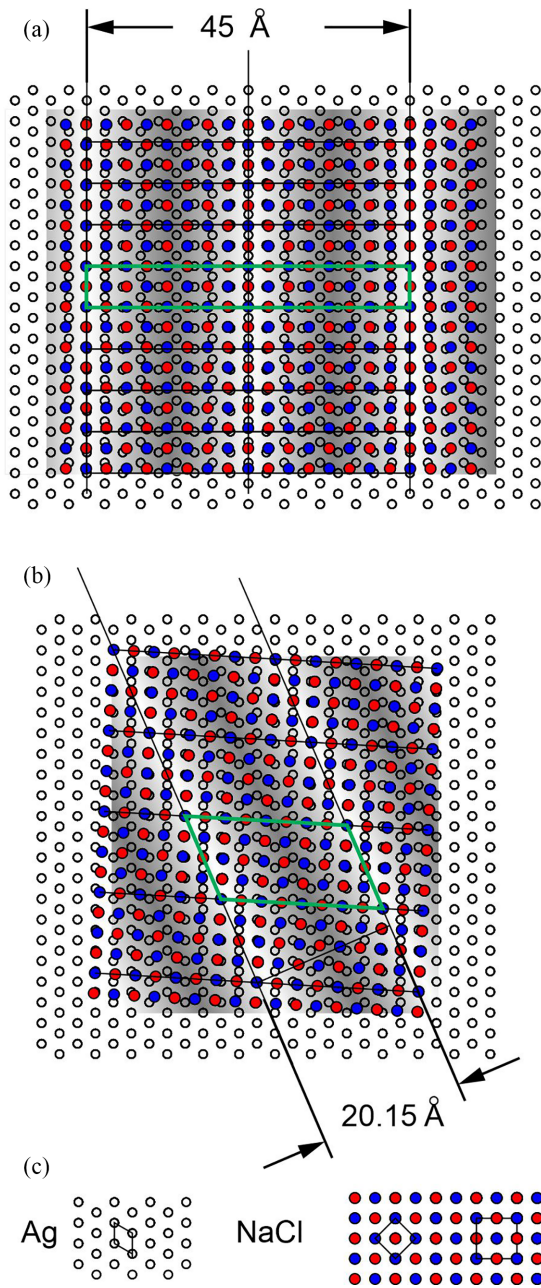


FIG. 2. Simplified models for the arrangement of NaCl on Ag(111) without relaxation of the atomic positions. Only the silver and the NaCl layer at the interface are shown. The silver atoms are given by the open circles, the Na⁺ ions by the red, and the Cl⁻ ions by the blue circles. (c) Hexagonal lattice of the silver and the square lattice of the NaCl. For the latter, both the primitive and the commonly used $c(\sqrt{2} \times \sqrt{2})$ unit cells are given. (a) If the lattices align, a $8\sqrt{2} \times \sqrt{2}$ superlattice is formed. A supercell is marked by the green rectangle. The shading indicates the alternating stripes of nearly top or bridge sites. (b) Tentative model for island II with a small rotation of the NaCl lattice relative to the silver lattice. A possible supercell is indicated in green.

in Fig. 2(a). It comprises two of the alternating stripes of nearly top or bridge sites. Hence, the observed period is $p = 22.5 \text{ \AA}$, half the length of the supercell. This type of island has a rectangular shape; the edges are given by the principal axis

of the NaCl lattice, one of them being aligned with an axis of the silver lattice. Density functional theory (DFT) calculations to understand the impact of the moiré pattern on the interface state are presented below.

Figure 2(b) yields a tentative model for the geometry of island II. It is more complicated because the square lattice of the NaCl is rotated by about 4° relative to the Ag lattice. Only a minimal distortion of the NaCl lattice is needed to form a commensurate supercell indicated by the green parallelogram. The period of the stripes is $p = 20.15 \text{ \AA}$, hence somewhat smaller than for island I. The shape of the island is irregular. The edges are partially aligned to the NaCl lattice, partially to the Ag lattice.

For all three islands of Fig. 1, a series of measurements for different tunneling voltages have been performed. The dI/dV images show a strong variation as a function of the tunneling voltage. In the following, we will focus on island II because the inclination of the moiré pattern relative to the sides of the islands helps to separate the observation of the modulation of the LDOS caused by the moiré pattern from the one resulting from reflections at the step edges.

Figure 3 shows for island II how the LDOS of the unoccupied states develops as a function of energy in steps of 0.1 eV between 0.23 eV and 0.43 eV. Only the data for five energies are displayed—the complete data set with all 21 images is given in the Appendix A. The gray scale represents the normalized differential conductance $\frac{dI}{dV} / \frac{I}{V}$ such that the absolute value as well as the variation of the measured dI/dV can be compared for the different tunneling voltages [29]. As can be seen, the average of the normalized differential conductance on the NaCl island continuously decreases with increasing energy. For further discussion of this data set, only the normalized conductance will be used.

The inner region of the island is dominated by a periodic modulation which exhibits exactly the same period for all energies. Superposed to this modulation and to be discussed in more detail below, the formation of standing waves in the vicinity of the edges can be seen. To disentangle the different modulations, the Fourier transform of each picture was calculated as displayed on the right side of Fig. 3. The dashed white circles mark the two spots which refer to the period of the pattern caused by the periodic potential. While their intensity may vary, their position is fixed, independent of the energy. The scattering at point defects within the island and the edges of the island leads to the more or less circular structure, which grows with increasing energy. It corresponds to the energy contour in k space.

To analyze the periodic modulation far from the edges, for each energy the average over a large area has been evaluated in Fig. 4. In the upper part of the figure, the direction and the area are indicated where the data were deduced. The average has been calculated over 550 lines perpendicular to the moiré pattern. In the middle of the figure, the line averages are displayed as a function of energy. To visualize the lateral modulation more clearly, the mean value has been subtracted for each energy. The blue horizontal line helps to visualize the change of the phase of the periodic pattern which occurs around $E = 0.265 \text{ eV}$. At bias voltages below 0.26 V, the maxima in the LDOS lie in the minima of the topography (where the surface appears less high in the STM image). In

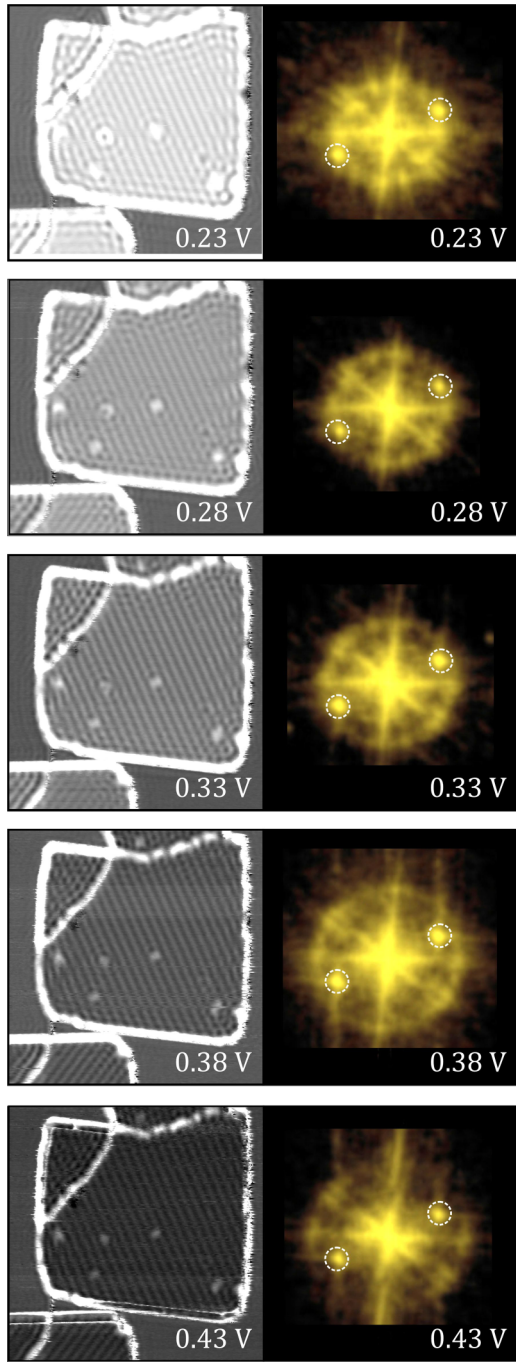


FIG. 3. $\frac{dI}{dV}/\frac{I}{V}$ measurements representing the density of states for island II at five different energies. The given voltages refer to the sample bias. The left side shows the real-space signal, the right side the corresponding Fourier transform. The latter indicates that the position of the two spots marked by the dashed white circles is independent of the energy. The full data set for 21 different energies is given in the Appendix A.

contrast, for bias voltages above 0.27 V, the maxima of the LDOS fall on the maxima of the topography. This is what one expects in case of a 1D nearly free electron gas and a periodic potential exhibiting a first band gap at around 0.265 eV. That implies that the maxima in the topography correspond

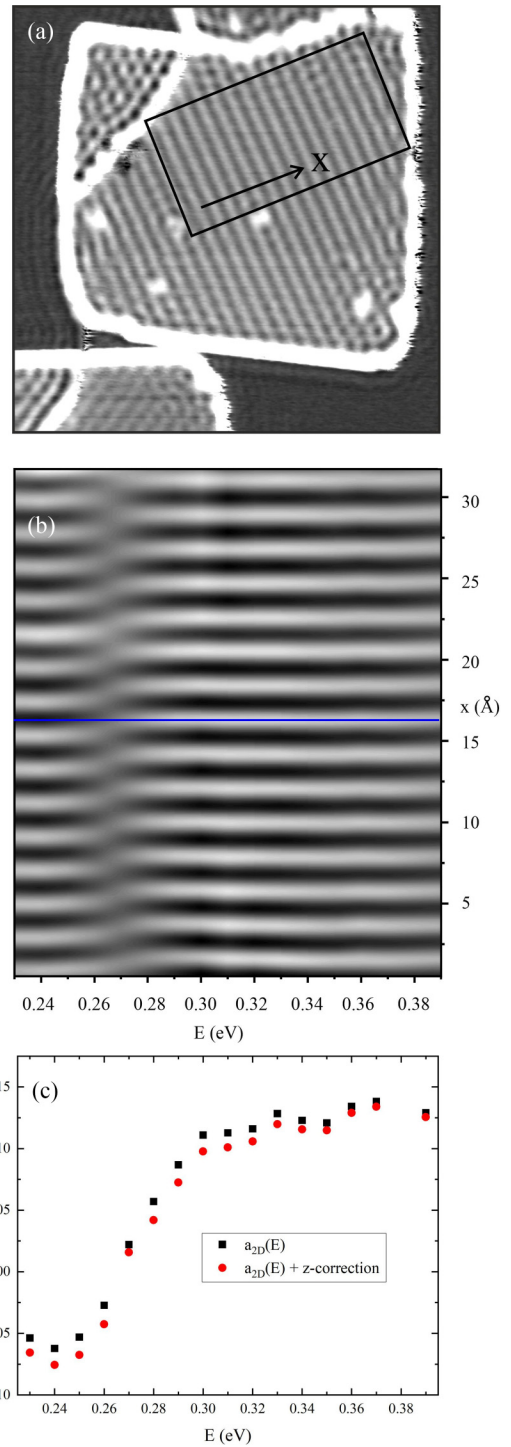


FIG. 4. Analysis of the dI/dV signal as function of position. (a) dI/dV data for island II at $E = 0.32$ eV. For further evaluation, the marked area has been selected and averaged along the rows. (b) The result as function of energy. (c) The corresponding modulation amplitude as function of energy. The black squares show the result without and the red dots with corrections, accounting for the small variation of the distance between the tunneling tip and the sample as function of the lateral position.

to maxima in the potential for the nearly free electron gas as well.

For further discussion, we consider the relative modulation of the LDOS as a function of the lateral position x ,

$$a(E) = \frac{\text{LDOS}(x = \frac{p}{2}) - \text{LDOS}(x = 0)}{\text{LDOS}(x = \frac{p}{2}) + \text{LDOS}(x = 0)}, \quad (1)$$

where we assume that the maxima and minima are located at the maximum and the minimum of the potential or vice versa. That leads to

$$\text{LDOS}(x, E) = \text{LDOS}_{\text{ave}}(E) \left[1 + a(E) \cos\left(\frac{2\pi}{p}x\right) \right], \quad (2)$$

where $\text{LDOS}_{\text{ave}}(E)$ is the LDOS averaged over (one period of) the periodic potential. For $a = 1$, it follows that $\text{LDOS}(x, E) \propto \cos^2(\frac{\pi}{p}x)$, for $a = -1$, $\text{LDOS}(x, E) \propto \sin^2(\frac{\pi}{p}x)$, and for $a = 0$, $\text{LDOS}(x, E)$ does not depend on x .

For a more quantitative comparison to the numerical calculations for each line $dI/dV \propto 1 + a_{2D}(E) \cos(\frac{2\pi}{p}x)$ has been fitted. The black squares in Fig. 4(c) display $a_{2D}(E)$ as a function of energy.

Since the images of dI/dV as a function of position are obtained in constant current operation of the STM, the distance between tip and sample is continuously readjusted to maintain a constant tunneling current. As can be seen in Fig. 1, there is a tiny periodic variation $\pm\Delta z$ with the periodicity of the moiré pattern because the total tunneling current is related to the integral over the density of electronic states from the Fermi level up to the energy given by the tunneling voltage according to Ref. [30]. Hence, for comparison to the numerical calculations performed for constant distance between tip and sample, a small correction of the data is required. Therefore, $\Delta z(E)$ was evaluated and the measured dI/dV data were multiplied by $f = e^{-2\alpha\Delta z(E)\cos(\frac{2\pi}{p}x)}$, where an estimated decay length of $\alpha = 1 \text{ \AA}^{-1}$ for the exponential distance dependence of the tunneling current is used. $\Delta z(E)$ slowly varies with the energy exhibiting at maximum $\pm 0.008 \text{ \AA}$ at $E = 0.27 \text{ eV}$. Hence, f is close to one, deviating by $\pm 1.6\%$ at maximum. The red dots in Fig. 4(c) show the corrected data for $a_{2D}(E)$ as a function of energy. This enhances the measured periodic modulation at energies below the gap of the subband and slightly reduces it above.

Figures 3 and 4 are deduced from a large area but only a limited set of energies. To obtain a complementary set of data, dI/dV curves as a function of energy but for a limited number of positions on the surface have been measured. Figure 5(a) displays several curves at positions near the maximum (red) or minimum (blue) of the lateral potential. As already found for the data set of Fig. 3, the average dI/dV signal decreases with growing energy above $E = 130 \text{ meV}$. In contrast to the data displayed in Figs. 3 and 4, the data have been acquired at constant distance between tip and sample but at various lateral positions while the tunneling voltage was swept. Figure 5(b) displays the aggregated information. The black line shows the average over two lateral periods. Again, for each energy, $\text{LDOS}(x, E) = \text{LDOS}_{\text{ave}}(E)[1 + a_{2D}(E) \cos(\frac{2\pi}{p}x)]$ has been evaluated. The red and blue curves show line sections of the obtained hypersurface for $x = 0$ and $x = p/2$. Figure 5(c) displays the relative modulation $a_{2D}(E)$.

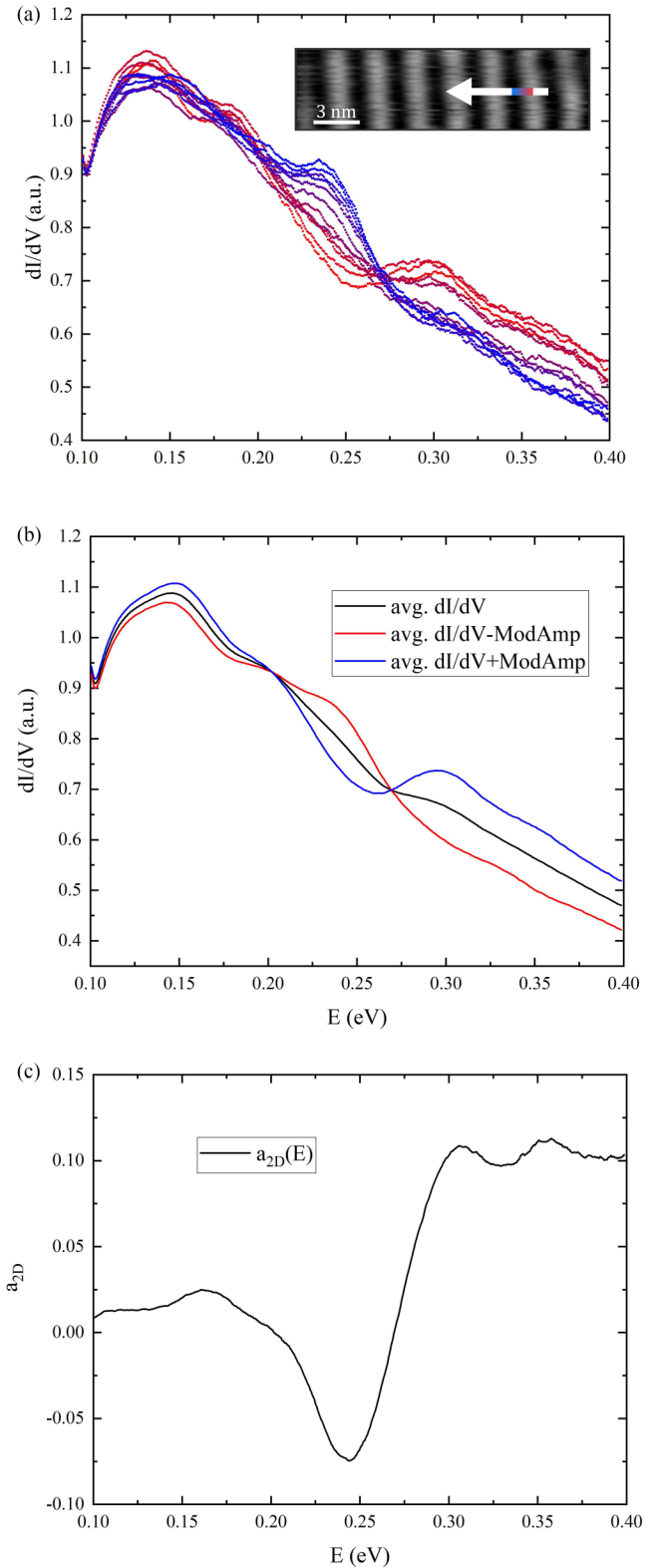


FIG. 5. (a) dI/dV measurements at 12 given positions—the position has been stepwise displaced along the arrow from the red to the blue position. (b) For the full data set along the arrow, the $\text{LDOS}(x, E)$ [Eq. (2)] was evaluated and the $\text{LDOS}(E)_{\text{ave}}$ is given by the black line. The red line shows $\text{LDOS}(E)_{\text{ave}}(1 + a_{2D}(E))$, the blue $\text{LDOS}(E)_{\text{ave}}(1 - a_{2D}(E))$. (c) Normalized modulation amplitude $a_{2D}(E)$.

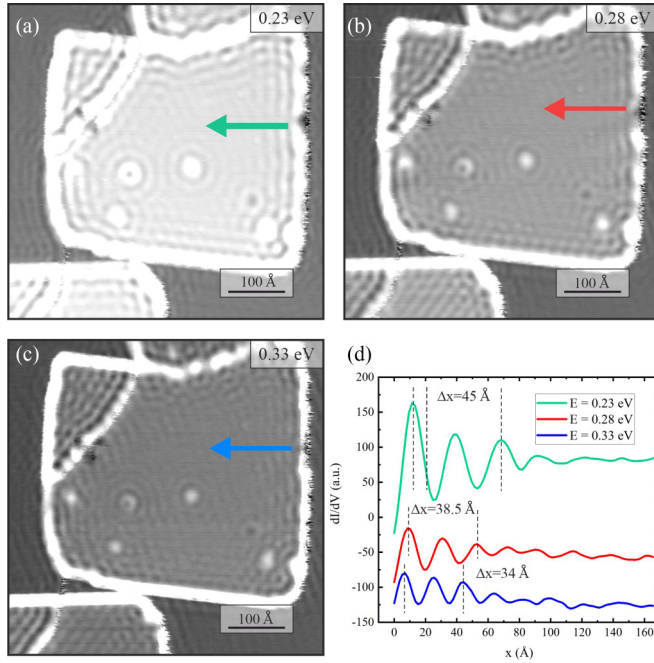


FIG. 6. Step edge induced modulation of the LDOS on the island of NaCl on Ag(111) studied in Figs. 3 and 4 at three different energies. To enhance the features, the effect of the periodic potential was removed by Fourier filtering. (a) at $E = 0.23$ eV, (b) at $E = 0.28$ eV, (c) at $E = 0.33$ eV. (d) Line scans along the lines indicated by the arrows. The change of the wavelength of the modulation as function of energy is clearly visible.

It is interesting to compare for the same NaCl island the modulation induced by the lattice mismatch with the silver to the standing wave patterns of the interface state caused by point defects and step edges. The experimental data, e.g., of Fig. 3, contain an incoherent superposition of both contributions. The part due to the periodic potential can be simply removed by suppressing the two spots in the Fourier transform of the data marked by the dashed white circles and transforming the data back in real space. For three energies, Fig. 6 displays the corresponding dI/dV patterns which clearly exhibit the characteristic features of standing electron waves. The line scans perpendicular to the right edge of the island shown in Fig. 6(d) reveal how the wavelength of the standing waves varies as a function of energy. The analysis for the full data set can be used to evaluate the dispersion relation for the interface state presented in Fig. 7. The onset of the latter was determined by dI/dV spectroscopy (see, e.g., Fig. 5) to $E_0 = 92$ meV. The blue curve is given by the relation $E(k) = E_0 + \frac{\hbar^2}{2m_{||}}k^2$. The best fit is obtained for an effective mass of $m_{||} = 0.56 m_e$ with the electron mass m_e , which is in good agreement with previous work [18,19,25]. A close inspection of the standing waves reveals a reduced coherence because the oscillations decay faster than expected for the ideal case, as the distance to the defect grows. According to Refs. [8,31], the modulation of the LDOS for limited coherence may be described by $\text{LDOS} \propto (1 - e^{-\frac{2x}{L_\Phi}} J_0(2k_0x))$, where J_0 is the zeroth Bessel function, x is the distance to the step edge, k_0 is the wave vector for the given energy, and L_Φ is the

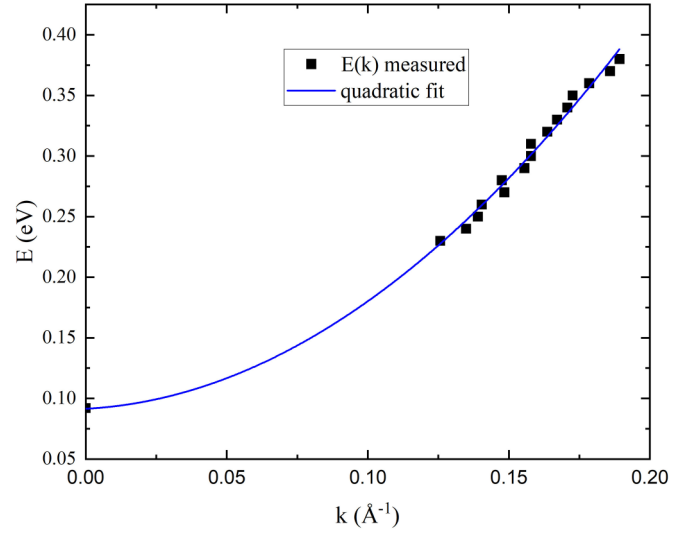


FIG. 7. $E(k)$ for the interface state as derived from the reflection at step edges.

phase coherence length. The comparison of calculations for different values to the experimental data provides a best fit for $L_\Phi \approx 100$ Å. As discussed below, this value will become important for the discussion of the modulation of the LDOS caused by the 1D periodic potential.

IV. THEORETICAL BACKGROUND

A. 1D

We first consider an electronic system subjected to a periodic potential $V(x)$ in one dimension. It can be described by a Bloch function

$$\psi_{n,k_x}(x) = e^{ik_x x} u_{n,k_x}(x), \quad (3)$$

where $u_{n,k_x}(x)$ is the periodic part of the Bloch function in x with an eigenvalue E_{n,k_x} for the energy; n denotes the electronic band, k_x is the wave vector. Due to its periodicity, the function can be expressed as a Fourier series,

$$u_{n,k_x}(x) = \sum_G C_{n,G}^{k_x} e^{-iGx}, \quad (4)$$

where $C_{n,G}^{k_x}$ are the coefficients for the Fourier component given by $G = 2\pi n_G/p$ with an integer number n_G and the period of the potential p . For an ideal system without defects, the local density of states will be given by

$$\begin{aligned} \text{LDOS}(x, E) &= \sum_{n,k_x} |u_{n,k_x}(x)|^2 \delta(E - E_{n,k_x}) \\ &= \sum_{n,k_x} \left(\sum_{G_1, G_2} C_{n,G_1}^{k_x*} C_{n,G_2}^{k_x} e^{i(G_1 - G_2)x} \right) \delta(E - E_{n,k_x}). \end{aligned} \quad (5)$$

We intentionally write the two summations separately because the inner sum represents the summation of the coherent contributions for a given energy and wave vector, whereas the outer sum incoherently adds the result of the inner sum for the different electronic bands and wave vectors.

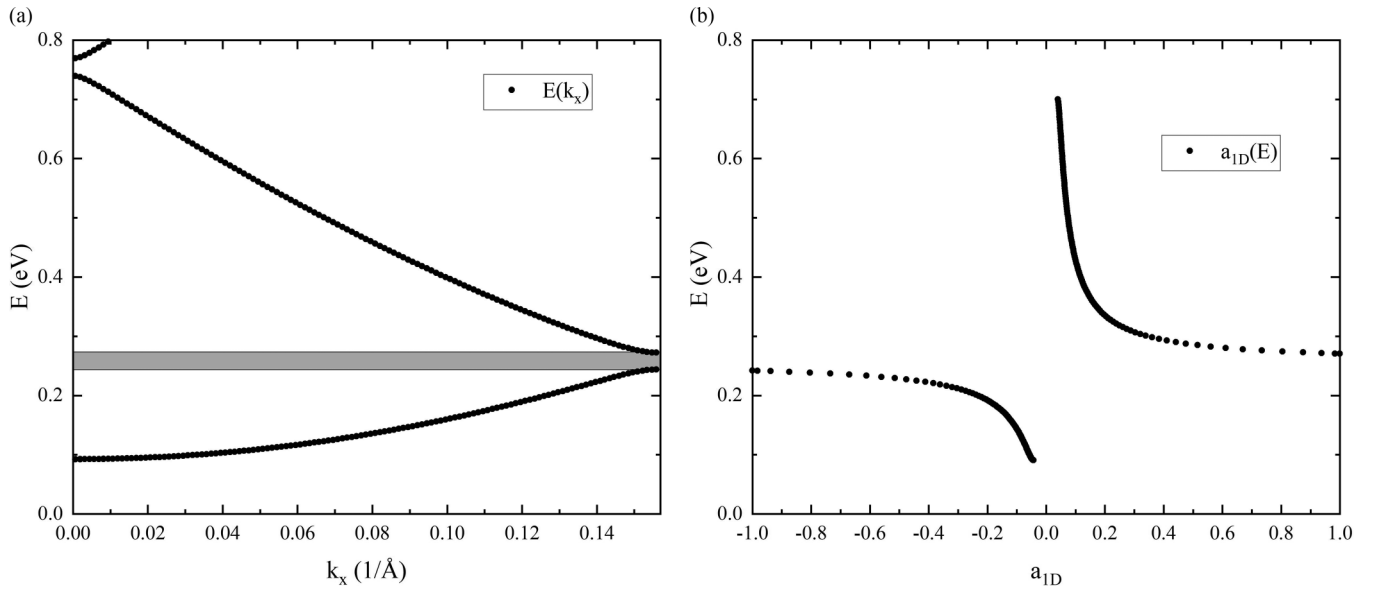


FIG. 8. (a) Energy versus k_x for a one-dimensional almost free electron subjected to a weak periodic potential for an effective mass $m_{\text{eff}} = 0.56m_e$, a period of $p = 20.15 \text{ \AA}$, and a potential height of $V_0 = 0.03 \text{ eV}$. The gray area indicates the first band gap. (b) a_{1D} versus energy. For energies below the gap, the modulation of the density of states as function of x is opposite in phase, above the gap in phase with the potential.

For a weak potential, bands separated by band gaps will be formed, see, e.g., the Kronig-Penney model [13]. Figure 8(a) shows the energy of the first two bands versus k_x for the first Brillouin zone as well as the band gap.

If we assume a periodic potential, which is symmetric around $x = 0$ and has its maximum at $x = 0$, e.g., $V = V_0 \cos(\frac{2\pi}{p}x)$, V_0 being the amplitude of the potential, the LDOS exhibits a periodic modulation in x . The modulation is small unless the energy is close to a band gap. To a good approximation it may be assumed to be sinusoidal.

For the relative modulation of the LDOS for the nearly free electron gas, one obtains $a_{1D}(E)$ displayed in Fig. 8(b) as function of energy. To facilitate the comparison to the experimental results, we have offset the energy by $E_0 = 0.092 \text{ eV}$, which is the energy of the band minimum of the interface state. As discussed in the Appendix B, the modulation is given to a good approximation by $a_{1D} \approx 2C_0^{k_x} C_{G=2\pi/p}^{k_x}$ (for $k_x > 0$). For energies below the first band gap, a_{1D} is negative, i.e., the maxima of the wave function and the LDOS lie in the minima of the potential. For energies above the gap, a_{1D} is positive.

B. 2D

If the electron gas is extended to two dimensions, we have $\vec{k} = (k_x, k_y)$. The solution of the Schroedinger equation is given by the product of two independent solutions $\psi(x, y) = \psi(x)\psi(y)$, where $\psi(x)$ is the wave function discussed above and $\psi(y)$ is the solution for a free electron. The band structure for k_x persists. The total energy is given by the sum

$$E_{n,\vec{k}} = E_x + E_y = E_{n,x}(k_x) + \frac{\hbar^2 k_y^2}{2m_{\parallel}}, \quad (6)$$

where $E_{n,x}(k_x)$ is the energy for the part of the solution in the x direction already discussed for the 1D case and m_{\parallel} is

the effective electron mass for the NFE. If the average over k vectors for a given total energy is considered, there is no band gap anymore because the y direction may contribute an arbitrary energy.

Figure 9(a) displays for energies below (blue dots) and above (red dots) the 1D band gap, pairs of k_x and k_y contributing to the LDOS. The new LDOS is the same as Eq. (5) with an extra summation over k_y . E_{n,k_x} is replaced by $E_{n,\vec{k}}$.

Figure 10 displays the LDOS as a function of position and energy obtained by solving the Schroedinger equation numerically. It reveals that at low energies only the coefficients $C_{n,G}^k$ with $G = -2\pi/p, 0, 2\pi/p$ contribute, leading to a period of p in the LDOS. For higher energy ($E > 0.27 \text{ eV}$), those contributions vanish and only coefficients for higher n contribute. The resulting modulation is relatively weak but it contains contributions of $G = 4\pi/p$ and $G = 6\pi/p$. For a consistent discussion, we will only consider the relative modulation of the LDOS, $a_{2D}(E)$ with a period p . Hence, $\text{LDOS} \propto 1 + a_{2D}(E) \cos(\frac{2\pi}{p}x)$. The continuous green line in Fig. 11 displays $a_{2D}(E)$ as a function of energy. For energies below the gap, it behaves rather similarly to the 1D case. It starts at almost zero and approaches a minimal value at an energy slight below the gap. However, in contrast to the 1D case, it stays close to zero and exhibits no maximum.

The results may be qualitatively understood by looking at the pairs of k_x and k_y selected by the delta function $\delta(E - E_{n,\vec{k}})$ in the extension to 2D of Eq. (5). They contribute with the $a_{1D}(E)$ corresponding to the k_x value. Figure 9(a) displays possible pairs of k_x and k_y in k space for an energy below (blue dots) and above (red dots) the first band gap (for k_x). It is important to note that for energies below the gap, E_x will be below the gap as well and all the pairs of k_x and k_y stem from the first band (for k_x), contributing to the LDOS with a negative a_{1D} . Figure 9(b) shows $a_{1D}(k_x)$ by the open blue

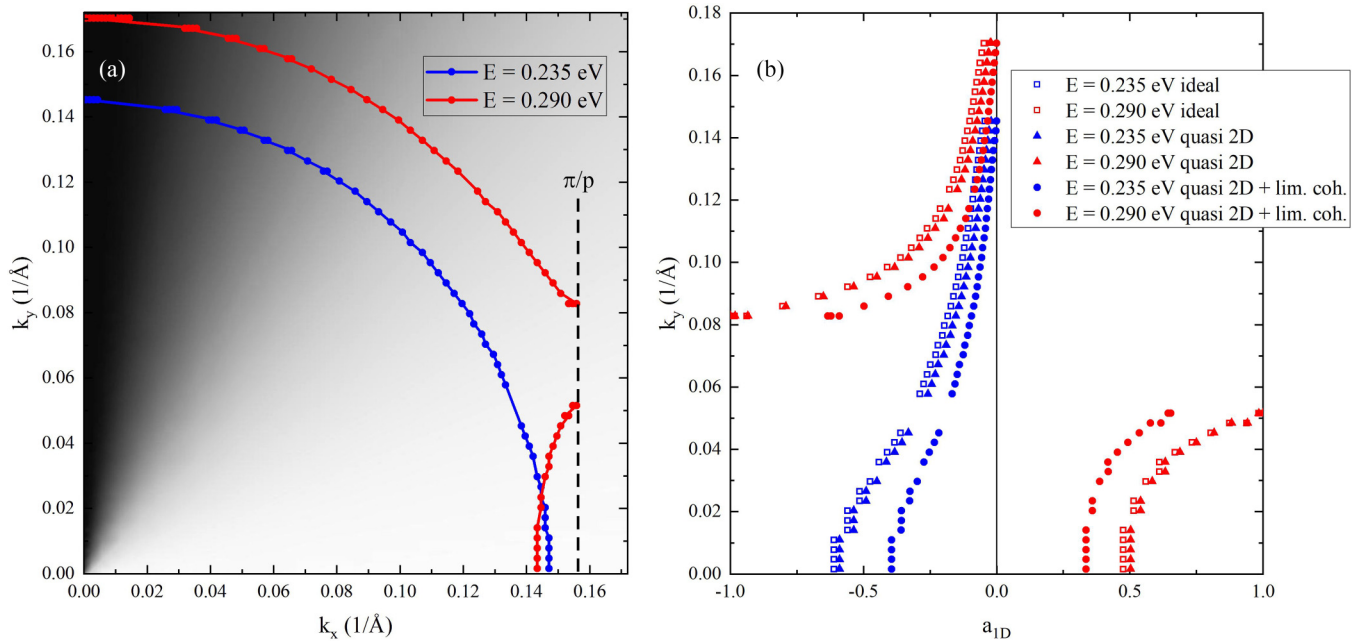


FIG. 9. (a) Pairs of k_x and k_y , below (blue) and above the first band gap (red), i.e., at energies of $E = 0.235$ eV and $E = 0.290$ eV. The continuous lines of constant energy were interpolated between the numerically calculated values. The underlying gray scale displays $P_{\text{coh}}(\vec{k})$, the weight for the contribution by the pair of k_x and k_y . (b) Contribution to the modulation by a_{1D} for the different k_y . The open squares display the results for the ideal 2D scenario, the filled triangles for the quasi-2D scenario, the full circles for the scenario including both the quasi-2D and the limited phase coherence.

squares. Hence, $a_{2D}(E)$ is negative and the LDOS will exhibit a modulation with a minimum at $x = 0$, as can be seen in the Figs. 10 and 11.

However, if the total energy is larger than the gap energy, the situation is more complex because E_x may be below or above the band gap. As a consequence, there are contributions

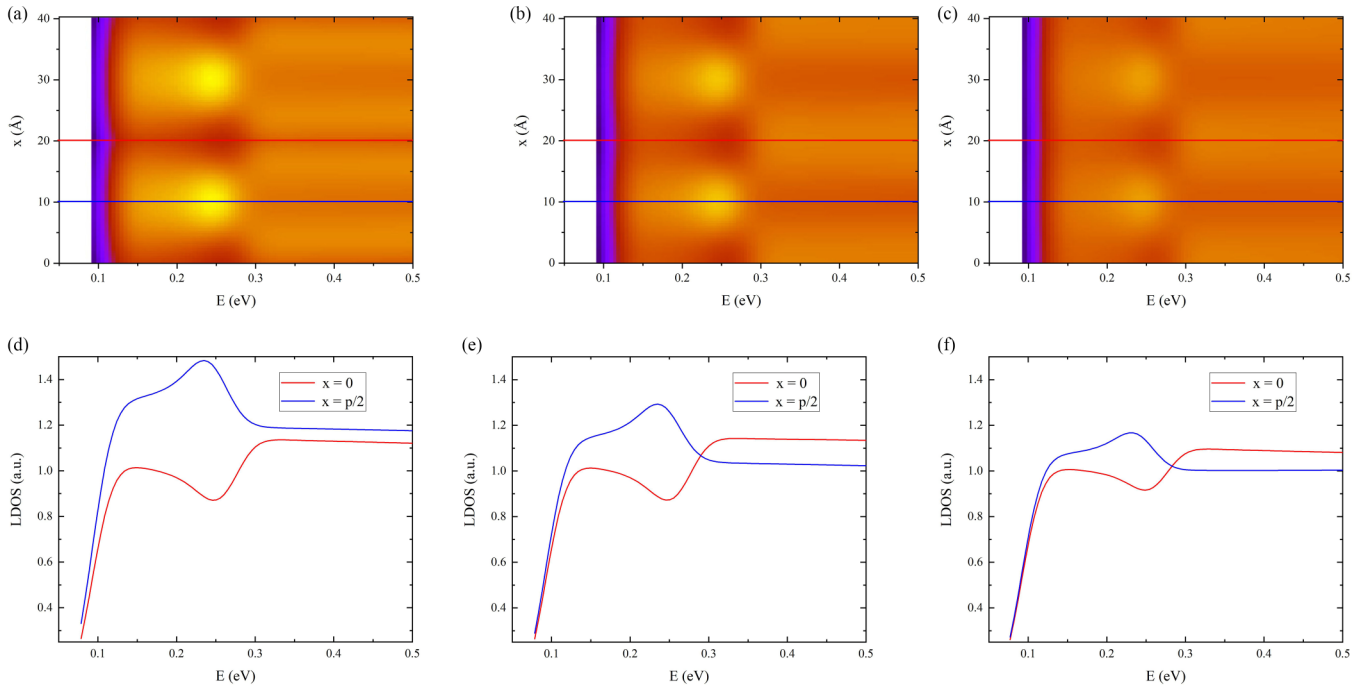


FIG. 10. Numerical calculation of the LDOS as function of lateral position and energy for the ideal 2D system (a), the quasi-2D system including the tunneling process (b), and the quasi-2D system, including the tunneling process and the limited phase coherence (c). (d)–(f) Corresponding line scans for each scenario on a maximum (red) and minimum (blue) of the periodic potential. For better comparison to the experimental data presented below, a band offset of $E_0 = 0.092$ meV has been included.

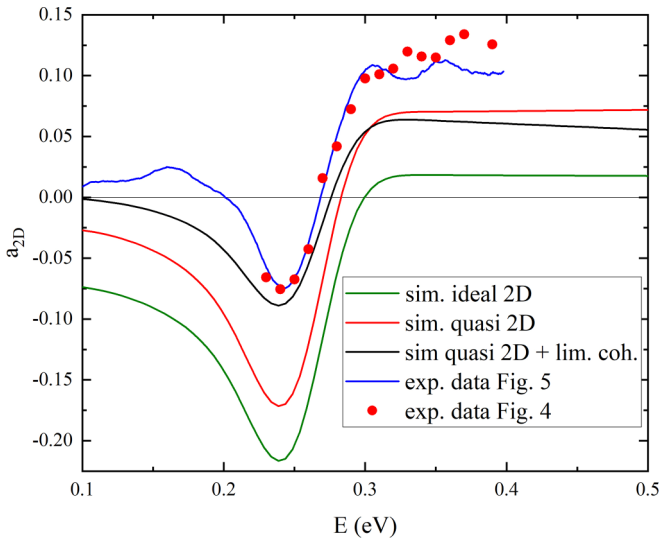


FIG. 11. Comparison between the numerical calculation of the modulation amplitude $a(E)$ of the LDOS as function of lateral position and energy for the ideal 2D system (green), the quasi-2D system including the tunneling process (red) and the quasi-2D system including the tunneling process and the limited phase coherence black line. The blue line displays the modulation according to Fig. 4, the red circles according to the data of Fig. 5.

to the sum in the LDOS from the first and the second bands, e.g. for $E = 0.29$ eV there are contributions from the first electronic band ranging from about $k_y = 0.08$ to 0.17 \AA^{-1} and from the second one ranging from about $k_y = 0$ to 0.06 \AA^{-1} , as indicated in Fig. 9(a) by the filled red circles. Figure 9(b) shows the value of $a_{1D}(E)$ for the different k_y . The contributions are strongest if k_x is close to the domain boundary. The part of the first band leads to a branch with negative sign, the one for the second band to a positive branch. For the ideal system, all pairs of k_x and k_y equally contribute and a calculation reveals that for energies above the band gap the modulation will almost vanish as shown in Figs. 10(a) and 10(d), and by the green line in Fig. 11.

However, the experimental results presented above reveal a modulation in the observed LDOS, which exhibits an about equal strength but an antiphase below and an in-phase contribution above the energy of the band gap.

C. Quasi-2D

In a physical experiment, the properties of a 2D system are observed if the system is confined in the third dimension to a narrow space above and below a plane. The LDOS shows a rapid decay with growing distance from this plane. In the presented experiment, the tip of a scanning tunneling microscope probes the LDOS in the exponential decay into the vacuum above the surface. Let us assume that the 2D electron system is confined to the plane $z = 0$, then the periodic part of the Bloch function $u_{n,\vec{k}}(x, z)$ contains exponentially decaying components in z which have to be included in the Fourier series. The vacuum side $z > 0$ is given by

$$u_{n,\vec{k}}(x, z) = \sum_G C_{n,G}^{k_x} e^{-iGx} e^{-\xi(G,\vec{k},E_{n,\vec{k}})|z|}. \quad (7)$$

The function decays exponentially with the decay coefficient $\xi(nG, \vec{k}, E_{n,\vec{k}})$, given by

$$\xi(G, \vec{k}, E_{\vec{k}}) = \sqrt{\frac{2m_{\perp}(e\phi - E_{n,\vec{k}})}{\hbar^2} + \frac{m_{\perp}}{m_{\parallel}}((k_x - G)^2 + k_y^2)}. \quad (8)$$

Here, ϕ is the work function, $E_{n,\vec{k}}$ is the band energy for the 2D electron state n, \vec{k} , m_{\perp} is the effective mass for the z coordinate, and m_{\parallel} for the x, y coordinates. The decay in z is a filter of high spatial frequencies since the second exponential in Eq. (7) rapidly decreases for larger values of G . This captures the typical effect of losing resolution as the STM tip moves away from the surface [30].

Figures 10(b) and 10(e) display the LDOS as calculated from Eq. (7) based on the numerical solution of the Schrodinger equation using $\phi = 3$ eV, $m_{\perp} = m_e$, and $m_{\parallel} = 0.56 m_e$ for a distance of 8 \AA between the tip and the sample surface, which roughly corresponds to the experimental parameters. The filtering of higher spatial frequencies is quite obvious, contributions for higher values of G are absent even for energies above the first band gap. Again, a lateral modulation of the LDOS is found which exhibits minima at the position of the maxima of the potential if the energy is below the band gap. However, now a lateral modulation of the LDOS is found, which is in phase with the potential for energies above the band gap, qualitatively recovering the features of the above experimental data.

The effect is due to the complex interplay of the contributions for $G = -2\pi/p, 0, 2\pi/p$. The lateral modulation of the LDOS is due to the interference term with the product for the two $G = 0$ and $G = 2\pi/p$ (or $G = -2\pi/p$ and $G = 0$). The contribution of the periodic potential affects the decay coefficient given by Eq. (8) for $G = \pm 2\pi/p$ such that it becomes smaller with increasing wave vector k_x and does not depend much on k_y (see Appendix C for details). As can be seen in Fig. 9(a) for energies above the band gap, there are contributions of the first band with k_x ranging from zero to the zone boundary and from the second band with k_x from some intermediate value to the zone boundary. Hence, as shown in Fig. 9(b) by the red triangles, the latter are less attenuated in average and the contributions no longer cancel. The modulation amplitude \bar{a}_{2D} as function of energy is plotted by the red curve in Fig. 11. The effect on the LDOS can also be seen Figs. 10(b) and 10(e).

Quantitatively, the experimental amplitude a_{2D} is larger than the one found with the above theory. One more effect is needed to account for the complete behavior of the experimental data.

D. Effect of limited spatial electronic coherence

It is well-known that in a real experiment the phase coherence will be limited. This has been discussed, e.g., for the Shockley-type electronic surface states on the noble metals [8,31,32]. The Fourier transform, Eq. (4), can be seen as the composition of electronic plane waves along the x direction. Indeed, it takes into account the scattering of the periodic potential and includes effects such as Bragg scattering. Electronic decoherence then will play a role in how these plane

waves compose. Let us use the reduced density matrix to study this [33]:

$$\hat{\rho}_k = \sum_{G_1, G_2} |k - G_1\rangle \langle k - G_2| \langle \Phi_{G_1}^k | \Phi_{G_2}^k \rangle. \quad (9)$$

This expression is based on the states $|k - G\rangle$ that correspond to each Fourier component of Eq. (4). However, the environment is included in the states $|\Phi_{G_2}^k\rangle$ that have to be taken into account to consider how interactions with the environment lead to decoherence of the 2D electronic state. Only when $G_1 \neq G_2$, the environment induces a change in the electronic state. Let us rename the coefficient to

$$\langle \Phi_{G_1+q}^k | \Phi_{G_2}^k \rangle = f(q, k), \quad (10)$$

such that $f(q = 0, k) = 1$.

Projecting the reduced density matrix in real space and taking into account the energy distribution of each state, we can evaluate the total local density of states that is used in the Tersoff-Hamman picture of STM [30]:

$$\begin{aligned} \text{LDOS}_T(x, y, E) = \sum_{n, \vec{k}} \left(\sum_{G_1, G_2} C_{G_1}^{k*} C_{G_2}^{k_x} e^{i(G_1 - G_2)x} \right. \\ \left. \times e^{-(\xi(G_1) + \xi(G_2))|z|} f(G_1 - G_2, k) \right) \\ \times \delta(E - E_{n, \vec{k}}). \end{aligned} \quad (11)$$

The observed LDOS mainly results from the lowest G values because the coefficients C_G^k are very small for higher G values (see Appendix B). Moreover, the higher spatial frequencies are damped by the stronger exponential decay into the vacuum.

Essentially, only the diagonal terms with $G_1 = G_2$ and $f(q = 0, k) = 1$ as well as the two off-diagonal pairs $G_1 - G_2 = \pm \frac{2\pi}{p}$ contribute. We set $P_{\text{coh}}(k) = \langle f_{G_1 \neq G_2, k} \rangle$ for the latter. Hence, the double sum over G in Eq. (11) can be separated in a diagonal ($G_1 = G_2$),

$$\begin{aligned} D_{n, \vec{k}} &= \sum_{G_1 = G_2} C_{G_1}^{k*} C_{G_2}^k e^{i(G_1 - G_2)x} e^{-(\xi(G_1) + \xi(G_2))|z|} \\ &= \sum_G |C_G^k|^2 e^{-2\xi(G)|z|}, \end{aligned} \quad (12)$$

and a nondiagonal ($G_1 \neq G_2$) part:

$$N_{n, \vec{k}} = \sum_{G_1 \neq G_2} C_{G_1}^{k*} C_{G_2}^k e^{i(G_1 - G_2)x} e^{-(\xi(G_1) + \xi(G_2))|z|}.$$

Finally, we obtain

$$\text{LDOS}_T(x, y, E) = \sum_{n, \vec{k}} (D_{n, \vec{k}} + P_{\text{coh}}(\vec{k}) N_{n, \vec{k}}) \delta(E - E_{n, \vec{k}}).$$

This may be rewritten, using the complete sum over the G 's:

$$\begin{aligned} \text{LDOS}_T(x, y, E) \\ = \sum_{n, \vec{k}} (P_{\text{coh}}(\vec{k}) S_{n, \vec{k}} + (1 - P_{\text{coh}}(\vec{k})) D_{n, \vec{k}}) \delta(E - E_{n, \vec{k}}), \end{aligned} \quad (13)$$

where $S_{n, \vec{k}} = D_{n, \vec{k}} + N_{n, \vec{k}}$. Hence, the resulting LDOS has a contribution given with the probability P_{coh} for a coherent process and one with the complementary probability $(1 - P_{\text{coh}})$ for processes with loss of coherence.

Phenomenologically, the different processes caused by the environment leading to a loss of the phase information can be accounted for by the phase coherent length L_Φ of an electron in the 2D state [31]. The interference of the wave functions causing the modulation of the LDOS by the periodic potential depends on the ratio between the period of the potential and the coherence length. Relevant is the effective coherence length given by the component of the coherence length perpendicular to the periodic potential $L_{\Phi, \text{eff}} = \frac{k_y}{|\vec{k}|} L_\Phi$. It is important to note that this leads to a different weight for the contributions to the oscillations of the LDOS, depending on the direction of the wave vector. Following Bürgi *et al.* [31] yields the probability for a coherent process,

$$P_{\text{coh}}(\vec{k}) = e^{-\frac{2p}{L_{\Phi, \text{eff}}}} = e^{-\frac{2p \sqrt{1 + \left(\frac{k_y}{k_x}\right)^2}}{L_\Phi}}, \quad (14)$$

where p is the period of potential $V(x)$ and L_Φ the phase coherence length. Figures 10(c) and 10(f) display the results of the numerical calculation using Eqs. (13) and (14). The coherence length has been estimated to $L_\Phi = 100 \text{ \AA}$ from the decay of the standing waves at step edges, as discussed above. The relative modulation amplitude \tilde{a}_{2D} as a function of energy is plotted by the black curve in Fig. 11. Obviously, the reduced coherence results in less interference, which is clearly visible below the energy gap. However, above the gap it merely affects the pattern which is out of phase with the modulation of the potential and the in-phase contribution dominates the incoherent sum. As a consequence, it exhibits an about equal negative and positive amplitude below and above the gap energy in agreement with the experimental observation, although the overall modulation amplitude is reduced because of the processes which destroy the coherence.

The findings for MgO on Au(111) [24] or NaCl on Cu(111) [20] and Ag(111) [18, 19, 25] have been mainly explained using the textbook models for a 1D electronic system with weak periodic potential. In contrast to the 1D model, it was observed that modulation of the LDOS with the period of the potential persists for a large range of energy above the band gap. This was attributed to the embedding of the 1D potential in the 2D electron gas. However, it was overlooked that this completely contradicts the prediction for an ideal system of this kind, which should show no modulation of the LDOS in that energy range at all.

E. DFT calculations

The numerical simulation of the modulation of the LDOS requires a model for the potential seen by the electrons of the interface state between Ag(111) and NaCl. To obtain an estimate for the magnitude of the potential, DFT calculations were performed. The VASP code was used with Projected Augmented Waves (PAW) atom potentials and the Perdew-Burke-Ernzerhof (PBE) exchange and correlation functional [34–36]. A $8\sqrt{2} \times \sqrt{2}$ unit cell was built on the Ag(111) surface to accommodate a NaCl bilayer. The size of the unit cell is determined by the mismatch of the respective lattice

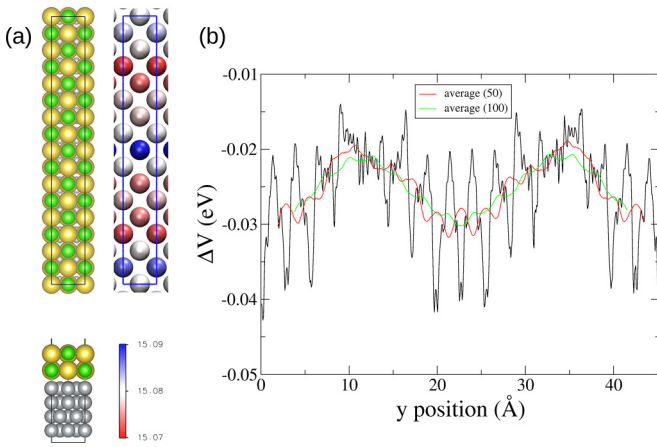


FIG. 12. DFT results of a NaCl bilayer on Ag(111). (a) NaCl layer corrugation due to the matching of the NaCl layer with the Ag(111) substrate. Despite the small value of the corrugation (~ 0.02 Å), there is a 1D potential created along the y axis by this corrugation. (b) One-electron potential created by the interaction of the NaCl bilayer with the Ag(111) substrate. (Compared to the model presented in Fig. 2 the x , and y axes are interchanged.)

parameters. Here, we used the PBE-DFT values for silver and NaCl, 4.08 Å and 3.99 Å, respectively. This is in agreement with the experimental observations above.

Figure 12(a) shows the periodic structure formed by the above unit cell. There is a natural 1D pattern along the x axis that is formed by the coincidence of Na and Cl atoms on certain Ag(111) sites. This leads to a physical corrugation of the layers as shown in Fig. 12. The potential induced by the NaCl layer on the electronic structure of Ag(111) is assumed to be due to the mutual interaction between layer and substrate. We evaluated it by taking the difference of the one-electron Kohn-Sham potential of the full system, NaCl on Ag(111), minus the potential of the NaCl layer, minus the potential of the Ag(111) substrate. This mutual potential is depicted in Fig. 12(b) and shows the period of the unit cell with a peak-to-peak value of ~ 10 meV, showing that a NaCl bilayer effect on the substrate's electronic layer is indeed in the range of tens of meV as assumed in the theory section.

V. DISCUSSION

The system NaCl on Ag(111) studied in this paper is one example for a nearly free 2D electron gas embedded in a 1D potential. Systems like the herringbone reconstruction of the Au(111) surface [15–17] or layers of organic molecules on Ag(111) [23] exhibit a strong corrugation, which makes it rather difficult to extract the LDOS from dI/dV measurements [22]. Islands of inorganic material like NaCl or MgO may grow on (111) surfaces of noble metals with very little corrugation manifesting in moiré patterns, which occur because large supercells are formed to accommodate the lattice mismatch. However, the accommodation of atoms of the adsorbate layer in different positions of the substrate causes a periodic potential which is important for the electronic interface state. Therefore, those systems are ideal to study the effect of a 1D potential on the nearly free electron gas of the interface state by scanning tunneling spectroscopy.

The findings for MgO on Au(111) [24] or NaCl on Cu(111) [20] and Ag(111) [18,19,25] have been mainly explained using the textbook models for a 1D electronic system with weak periodic potential. In contrast to the 1D model, it was observed that modulation of the LDOS with the period of the potential persists for a large range of energy above the band gap. This was attributed to the embedding of the 1D potential in the 2D electron gas. However, it was overlooked that this completely contradicts the prediction for an ideal system of this kind, which should show almost no modulation of the LDOS in that energy range at all.

The presented theoretical description of the 2D system shows that to explain the observation by us and other groups as well, the detection mechanism by the tunneling microscope and the limited spatial coherence need to be included. According to Refs. [8,37], the main cause for the latter is the electron-electron scattering. The tunneling process and the decoherence favor the contributions to the LDOS which correspond to the LDOS of the purely 1D system. In particular, it explains why for energies above the band gap the modulation of the LDOS with maxima on the maxima of the 1D potential is not canceled by the contribution from wave vectors with a component mainly parallel to the valleys or ridges of the potential. Based on the numerical solutions of the Schrodinger equation, the LDOS to be observed by the tip of the STM has been calculated, including the spatial coherence length. The latter was evaluated from the decay of standing electron waves at step edges to $L_\Phi \approx 100$ Å. Figure 11 shows the comparison between the numerical calculations of the modulation amplitude for the different scenarios sketched above (green, red, and black lines) and the experimental results based on dI/dV measurements presented in Figs. 4 and 5 (red dots and blue line). The green line displays the ideal 2D system predicting that there should be almost no visible modulation for energies above the band gap. For the red line, the spatial filtering by the tunneling process between the tunneling tip and the sample has been accounted for. Finally, the black line displays the calculations including, in addition, the limited spatial coherence. The experimental results extracted from the data shown in Fig. 4 are given by the red dots, those from the data of Fig. 5 by the continuous blue line. The agreement is not perfect, but the essential features of the experiment are reproduced. The comparison to the experimental observation provides the best agreement for a modulation of the periodic potential of about $\Delta E_{p-p} = 30$ meV. This is about the same magnitude as given by the DFT calculations as well as the potential for the surface state found on the herringbone reconstruction of the Au(111) surface [38].

The moiré pattern of NaCl islands exhibits different periods and orientations depending on island size and other parameters which are related to the dynamic of the growth. For the present paper, we focused on a NaCl island on Ag(111) which is large enough to observe the modulation of the LDOS far from the edges and which exhibits a periodic potential that is not oriented parallel to one of the edges. See Supplemental Material [39] for the calculation of the standing waves caused by step edges in the presence of a periodic potential at an arbitrary angle. Hence, the interplay between standing waves of the 2D electrons caused by scattering at any kind of defects, like point defects or step edges, and the

modulation of the LDOS exhibiting the period of the potential which is observed for the infinite and defect-free system can be disentangled. The first type occurs for all energies above the band onset except the mini band gap caused by the periodic potential, and shows the dispersion $E(k)$ of the nearly free electron gas, while the second is dispersionless. For systems of finite size, it can be difficult to distinguish the different contributions. This has led to the false conclusion [24] that this electronic state shows the normal parabolic dispersion below the band gap and no dispersion above, leading to a vertical line in the $E(k)$ diagram.

VI. SUMMARY

The investigation of the LDOS of a 2D system subjected to a 1D periodic potential reveals two kinds of modulations. One type is caused by the interaction with defects, e.g., point or line defects. They reveal an energy-dependent period which is described by the dispersion relation of the 2D state. In contrast for a defect-free system, the LDOS exhibits a periodic modulation with a period of the periodic potential which is independent of the electron energy. Our experimental results confirm a series of observations for a nearly free 2D electron gas interacting with a 1D periodic potential, e.g., for the herringbone reconstruction on Au(111), MgO islands on Au(111) [24], or NaCl islands on Cu(111) [20]. The interaction leads to the formation of subbands and a periodic modulation of the density of states found for energies below and above the corresponding band gap. As one would expect for a pure 1D system, for energies below the gap the maxima in the LDOS are located between the maxima of the periodic potential and on the maxima for energies above. However, the latter observation contradicts the prediction for an ideal 2D system because the out-of-phase and in-phase contributions should almost cancel. To explain the discrepancy, different effects have to be considered. The observation by scanning tunneling spectroscopy leads to a filtered result because the tunneling probability for electrons depends on the wave vector of the electrons. That leads to the reduction of contributions at higher spatial frequencies slightly enhancing the 1D character of the system. However, the effect is too small to fully explain the observations. We propose that the apparent one-dimensionality of these systems is largely caused by the limited spatial phase coherence of the electronic states. This reduces the contribution of k vectors with the major component parallel to the rows. This can also be interpreted as a longer effective path for the interference between the rows of the periodic potential.

In short, for an ideal system, such a periodic modulation should only be found below the band gap of the subbands caused by the periodic potential. However, the experimental observation reveals an even stronger modulation above the gap. This can be explained if the limited phase coherence is included in the description of the processes.

ACKNOWLEDGMENTS

K.K. and R.M. thank the Deutsche Forschungsgemeinschaft (DFG, German Research Foundation) for funding

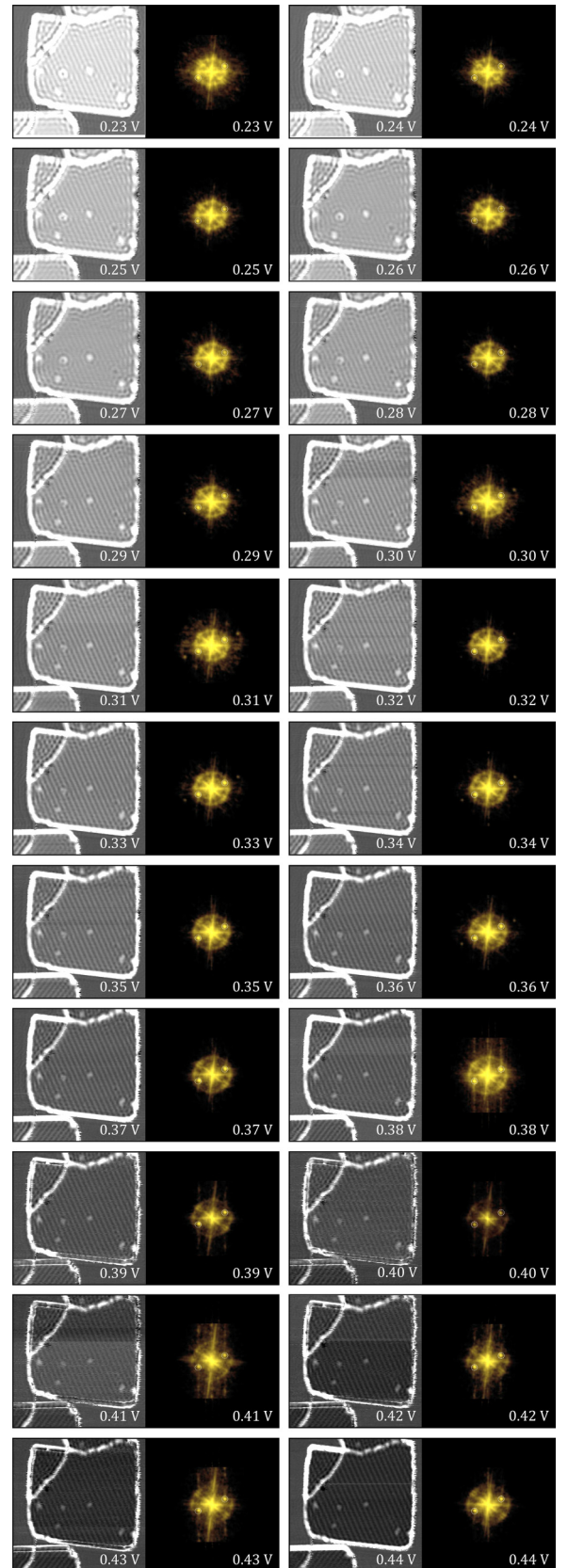


FIG. 13. Full data set of dI/dV measurements for island II. The given voltages refer to the sample bias.

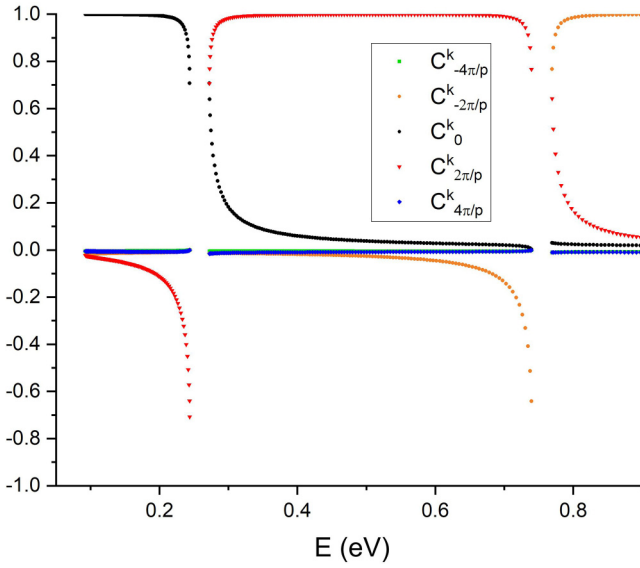


FIG. 14. The coefficients $C_G^{k_x}$ as function of energy for the 1D case.

through Project No. 278162697–SFB 1242. R.R. and N.L. acknowledge financial support from the Spanish State Research Agency Grant No. PID2021-127917NB-I00 funded by MCIN/AEI/10.13039/501100011033 and by “ERDF A way of making Europe”; and they are grateful for the computer resources at Finisterrae II, and the technical support provided by CESGA. The authors would like to thank J. König and K. Hornberger, University of Duisburg-Essen for invaluable discussions.

APPENDIX A: FULL DATA SET OF DI/DV IMAGES OF ISLAND II

Figure 13 shows the LDOS of the unoccupied states for island II as a function of energy in steps of 0.1 eV between 0.23 eV and 0.43 eV. The gray scale represents the normalized differential conductance $dI/dV / IV$. The corresponding Fourier transform of each picture is displayed on the right side of each subfigure.

APPENDIX B: APPROXIMATE RELATION BETWEEN THE $C_G^{k_x}$ AND a_{1D}

To understand the observations, it is helpful to look at the interplay of the coefficients $C_G^{k_x}$. It should be noted that for the given symmetry, the imaginary part is zero. Hence, it is sufficient to consider the real part. Furthermore, we restrict the wave vector to $k_x > 0$. The values for $k_x < 0$ are obtained by interchanging G and $-G$. Figure 14 displays the coefficients for $G = -\frac{4\pi}{p}, -\frac{2\pi}{p}, 0, \frac{2\pi}{p}, \frac{4\pi}{p}$ as a function of energy for the first, the second, and the beginning of the third band.

For the following discussion, we set $\tilde{G} = \frac{2\pi}{p}$. As can be seen to a good approximation, only $C_0^{k_x}$ and $C_{\tilde{G}}^{k_x}$ contribute. Hence, one obtains

$$|u_{n,k_x}(x)|^2 = |C_0^{k_x} + C_{\tilde{G}}^{k_x} e^{-i\tilde{G}x}|^2 \quad (\text{B1})$$

$$= |C_0^{k_x} e^{i\frac{\tilde{G}}{2}x} + C_{\tilde{G}}^{k_x} e^{-i\frac{\tilde{G}}{2}x}|^2 \quad (\text{B2})$$

$$= (C_0^{k_x})^2 + (C_{\tilde{G}}^{k_x})^2 + C_0^{k_x} C_{\tilde{G}}^{k_x} e^{i\tilde{G}x} + C_0^{k_x} C_{\tilde{G}}^{k_x} e^{-i\tilde{G}x} \quad (\text{B3})$$

$$= (C_0^{k_x})^2 + (C_{\tilde{G}}^{k_x})^2 + 2C_0^{k_x} C_{\tilde{G}}^{k_x} \cos \tilde{G}x. \quad (\text{B4})$$

In consequence, only the interference term $2C_0^{k_x} C_{\tilde{G}}^{k_x} \cos \tilde{G}x$ leads to a modulation of the LDOS. To understand the origin of the modulation as function of x , it is to a good approximation sufficient to consider the product $2C_0^{k_x} C_{\tilde{G}}^{k_x}$. For the 1D situation, it directly follows that $a_{1D} = 2C_0^{k_x} C_{\tilde{G}}^{k_x}$. For $n = 1$, it is negative and approaches -1 when the energy approaches the first band gap. For $n = 2$, it is positive, starts with $+1$ at the band edge, and decreases with growing energy. It should be noted that the same is obtained for negative k_x by replacing $C_{\tilde{G}}^{k_x}$ by $C_{-\tilde{G}}^{k_x}$.

APPENDIX C: ATTENUATION OF THE CONTRIBUTION TO THE MODULATION OF THE LDOS BY THE DECAY OF THE WAVE FUNCTION INTO THE VACUUM

By placing $E_{n,\vec{k}}$ from Eq. (6) into Eq. (8), one finds for the exponent describing the decay into the vacuum:

$$\xi(G, \vec{k}, E_{\vec{k}}) = \sqrt{\frac{2m_{\perp}(e\phi - (E_{n,k_x} - \frac{\hbar^2 k_x^2}{2m_{\parallel}}))}{\hbar^2} - 2\frac{m_{\perp}}{m_{\parallel}}k_x G + \frac{m_{\perp}}{m_{\parallel}}G^2}.$$

For a nearly free electron system, $\delta(k_x) = (E_{n,k_x} - \frac{\hbar^2 k_x^2}{2m_{\parallel}})$ will be small and the major variation of ξ as function of k_x results from the term $-2\frac{m_{\perp}}{m_{\parallel}}k_x G$. Based on the approximate relation between the $C_{nG}^{k_x}$ and a_{1D} discussed above, to first approximation the effect of ξ needs to be considered only for $G = 0$ and $G = 2\pi/p$ or $G = 0$ and $G = -\frac{2\pi}{p}$ for $k_x < 0$. As can be seen from the formula, k_x and $-k_x$ will yield the same ξ . Hence, the contribution to the modulation of the LDOS

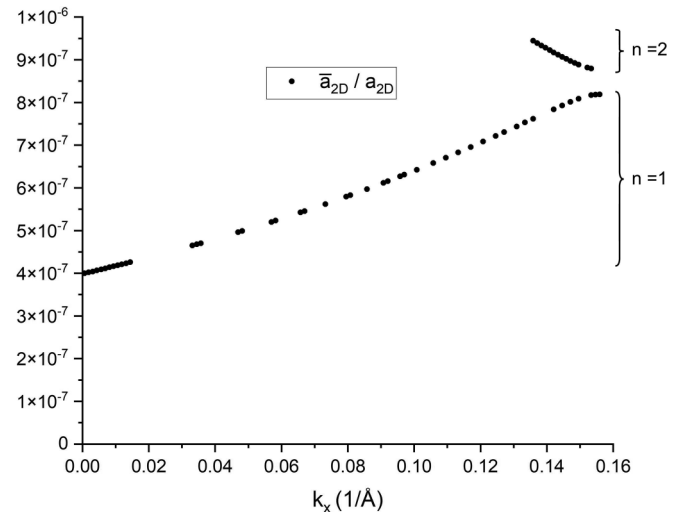


FIG. 15. Ratio \bar{a}_{1D}/a_{1D} as a function of k_x for an energy of $E = 0.305$ eV.

boils down to

$$\bar{a}_{1D} \approx 2C_0^{k_x} C_G^{k_x} e^{-(\xi(G=0, k_x) + \xi(G=\frac{2\pi}{p}, k_x))z}.$$

Since approximately $\xi(G=0, k_x)$ does not depend on k_x , one obtains for the attenuation by the tunneling junction:

$$\bar{a}_{1D}/a_{1D} \propto e^{\frac{2m_{\parallel}}{m_{\perp}} k_x n G z}.$$

Figure 15 shows the ratio \bar{a}_{1D}/a_{1D} of the full calculation as a function of k_x for the pairs of k_x and k_y for $E = 0.305$ eV from Fig. 9. It displays the exponential increase with increasing k_x predicted by the approximation above. Only close to the energy of the band gap, deviations due to $\delta(k_x)$ become significant. As a consequence, the negative contribution from the first band to a_{2D} for small k_x has less weight than the positive one of the second band at higher k_x . Hence, a modulation of the LDOS in phase with the modulation of the potential is predicted for electron energies above the first band gap.

-
- [1] M. J. Kelly, The two-dimensional electron gas subject to a weak periodic potential, *J. Phys. C* **18**, 6341 (1985).
- [2] K. P. D. Weiss, K. v. Klitzing and G. Weimann, Magnetoresistance oscillations in a two-dimensional electron gas induce by a submicrometer periodic potential, *Europhys. Lett.* **8**, 179 (1989).
- [3] A. K. Das, M. L. Glasser, and S. H. Payne, On a two-dimensional electron gas modulated by a periodic potential, *J. Phys. C* **21**, 357 (1988).
- [4] H. L. Stormer, L. N. Pfeiffer, K. W. Baldwin, K. W. West, and J. Spector, Atomically precise superlattice potential imposed on a two-dimensional electron gas, *Appl. Phys. Lett.* **58**, 726 (1991).
- [5] M. F. Crommie, C. P. Lutz, and D. M. Eigler, Imaging standing waves in a two-dimensional electron gas, *Nature (London)* **363**, 524 (1993).
- [6] Y. Hasegawa and P. Avouris, Direct Observation of Standing Wave Formation at Surface Steps Using Scanning Tunneling Spectroscopy, *Phys. Rev. Lett.* **71**, 1071 (1993).
- [7] J. Li, W.-D. Schneider, R. Berndt, and S. Crampin, Electron Confinement to Nanoscale Ag Islands on Ag(111): A Quantitative Study, *Phys. Rev. Lett.* **80**, 3332 (1998).
- [8] L. Bürgi, N. Knorr, H. Brune, M. Schneider, and K. Kern, Two-dimensional electron gas at noble-metal surfaces, *Appl. Phys. A* **75**, 141 (2002).
- [9] K. S. Novoselov, V. I. Fal'ko, L. Colombo, P. R. Gellert, M. G. Schwab, and K. Kim, A roadmap for graphene, *Nature (London)* **490**, 192 (2012).
- [10] K. Reidy, G. Varnavides, J. D. Thomsen, A. Kumar, T. Pham, A. M. Blackburn, P. Anikeeva, P. Narang, J. M. LeBeau, and F. M. Ross, Direct imaging and electronic structure modulation of moiré superlattices at the 2D/3D interface, *Nat. Commun.* **12**, 1290 (2021).
- [11] L. Zhou, L. Liao, J. Wang, J. Yu, D. Li, Q. Xie, Z. Liu, Y. Yang, X. Guo, and Z. Liu, Substrate-induced graphene chemistry for 2D superlattices with tunable periodicities, *Adv. Mater.* **28**, 2148 (2015).
- [12] C. Zhang, C.-P. Chuu, X. Ren, M.-Y. Li, L.-J. Li, C. Jin, M.-Y. Chou, and C.-K. Shih, Interlayer couplings, moiré patterns, and 2D electronic superlattices in MoS₂/WSe₂ hetero-bilayers, *Sci. Adv.* **3**, e1601459 (2017).
- [13] R. de L. Kronig and W. G. Penney, Quantum mechanics of electrons in crystal lattices, *Proc. R. Soc. London A* **130**, 499 (1931).
- [14] B. G. Briner, P. Hofmann, M. Doering, H.-P. Rust, E. W. Plummer, and A. M. Bradshaw, Observation of interfering Bloch waves, *Europhys. Lett.* **39**, 67 (1997).
- [15] L. Petersen, P. Laitenberger, E. Lægsgaard, and F. Besenbacher, Screening waves from steps and defects on Cu(111) and Au(111) imaged with STM: Contribution from bulk electrons, *Phys. Rev. B* **58**, 7361 (1998).
- [16] K. Lauwaet, K. Schouteden, E. Janssens, C. V. Haesendonck, and P. Lievens, Dependence of the NaCl/Au(111) interface state on the thickness of the NaCl layer, *J. Phys.: Condens. Matter* **24**, 475507 (2012).
- [17] K. Lauwaet, K. Schouteden, E. Janssens, C. Van Haesendonck, P. Lievens, M. I. Trioni, L. Giordano, and G. Pacchioni, Resolving all atoms of an alkali halide via nanomodulation of the thin NaCl film surface using the Au(111) reconstruction, *Phys. Rev. B* **85**, 245440 (2012).
- [18] S.-C. Heidorn, A. Sabellek, and K. Morgenstern, Size dependence of the dispersion relation for the interface state between NaCl(100) and Ag(111), *Nano Lett.* **14**, 13 (2014).
- [19] S. Heidorn, B. Gerss, and K. Morgenstern, Step edge induced reconstructions of NaCl(100) bilayers on Ag(111): A route to alter the properties of nanoscale insulators, *ACS Appl. Nano Mater.* **1**, 6818 (2018).
- [20] J. Repp, G. Meyer, and K.-H. Rieder, Snell's Law for Surface Electrons: Refraction of an Electron Gas Imaged in Real Space, *Phys. Rev. Lett.* **92**, 036803 (2004).
- [21] N. Gonzalez-Lakunza, I. Fernández-Torrente, K. J. Franke, N. Lorente, A. Arnau, and J. I. Pascual, Formation of Dispersive Hybrid Bands at an Organic-Metal Interface, *Phys. Rev. Lett.* **100**, 156805 (2008).
- [22] A. Sabitova, R. Temirov, and F. S. Tautz, Lateral scattering potential of the PTCDA/Ag(111) interface state, *Phys. Rev. B* **98**, 205429 (2018).
- [23] L. Eschmann, A. Sabitova, R. Temirov, F. S. Tautz, P. Krüger, and M. Rohlfing, Coverage-dependent anisotropy of the NTCDA/Ag(111) interface state dispersion, *Phys. Rev. B* **100**, 125155 (2019).
- [24] Y. Pan, S. Benedetti, N. Nilius, and H.-J. Freund, Change of the surface electronic structure of Au(111) by a monolayer MgO(001) film, *Phys. Rev. B* **84**, 075456 (2011).
- [25] S. Heidorn, C. Bertram, J. Koch, K. Boom, F. Matthaiei, A. Safiei, J. Henzl, and K. Morgenstern, Influence of substrate surface-induced defects on the interface state between NaCl(100) and Ag(111), *J. Phys. Chem. C* **117**, 16095 (2013).
- [26] P. Zahl, M. Bierkandt, S. Schröder, and A. Klust, The flexible and modern open source scanning probe microscopy software package GXSM, *Rev. Sci. Instrum.* **74**, 1222 (2003).
- [27] I. Horcas, R. Fernández, J. M. Gómez-Rodríguez, J. Colchero, J. Gómez-Herrero, and A. M. Baro, WSXM: A software for

- scanning probe microscopy and a tool for nanotechnology, *Rev. Sci. Instrum.* **78**, 013705 (2007).
- [28] C. A. Schneider, W. S. Rasband, and K. W. Eliceiri, NIH image to ImageJ: 25 years of image analysis, *Nat. Methods* **9**, 671 (2012).
- [29] R. Feenstra, J. A. Stroscio, and A. Fein, Tunneling spectroscopy of the Si(111)2x1 surface, *Surf. Sci.* **181**, 295 (1987).
- [30] J. Tersoff and D. R. Hamann, Theory of the scanning tunneling microscope, *Phys. Rev. B* **31**, 805 (1985).
- [31] L. Bürgi, O. Jeandupeux, H. Brune, and K. Kern, Probing Hot-Electron Dynamics at Surfaces with a Cold Scanning Tunneling Microscope, *Phys. Rev. Lett.* **82**, 4516 (1999).
- [32] L. Vitali, P. Wahl, M. Schneider, K. Kern, V. Silkin, E. Chulkov, and P. Echenique, Inter- and intraband inelastic scattering of hot surface state electrons at the Ag(111) surface, *Surf. Sci.* **523**, L47 (2003).
- [33] P. Schattschneider and S. Löffler, Entanglement and decoherence in electron microscopy, *Ultramicroscopy* **190**, 39 (2018).
- [34] G. Kresse and J. Furthmüller, Efficiency of *ab-initio* total energy calculations for metals and semiconductors using a plane-wave basis set, *Comput. Mater. Sci.* **6**, 15 (1996).
- [35] G. Kresse and J. Furthmüller, Efficient iterative schemes for *ab initio* total-energy calculations using a plane-wave basis set, *Phys. Rev. B* **54**, 11169 (1996).
- [36] G. Kresse and D. Joubert, From ultrasoft pseudopotentials to the projector augmented-wave method, *Phys. Rev. B* **59**, 1758 (1999).
- [37] M. Bauer, A. Marienfeld, and M. Aeschlimann, Hot electron lifetimes in metals probed by time-resolved two-photon photoemission, *Prog. Surf. Sci.* **90**, 319 (2015).
- [38] L. Bürgi, H. Brune, and K. Kern, Imaging of Electron Potential Landscapes on Au(111), *Phys. Rev. Lett.* **89**, 176801 (2002).
- [39] See Supplemental Material at <http://link.aps.org/supplemental/10.1103/PhysRevB.107.155418> for a mathematical description of the modulation of the local density of states caused by a step edge for two-dimensional electron system modulated by a weak one-dimensional periodic potential of arbitrary orientation.